The Role Played by Current Phase Shift on Magnetic Field Established by AC Double-Circuit Overhead Transmission Lines—Part I: Static Analysis

Giovanni Mazzanti, *Member, IEEE*

***Abstract*—AC double-circuit overhead transmission lines may exhibit large phase-shift angles between current phasor terns of the two circuits. Here, a static analysis (relevant to single time instants or constant load conditions) of the role played by such a phase shift on the magnetic field established by these lines is performed, showing that the phase-shift angle interacts with the phase conductor arrangement, resulting in a wide variety of field profiles at a given line section. The analysis, carried out for two tower topologies and several couples of rms current values, reveals interesting general features of field profiles that depend only on the phase-shift angle. This proves that neglecting, or even misunderstanding, current phase-shift effects for ac double-circuit overhead transmission lines can lead to severe errors in field calculation that may have negative consequences on human exposure estimates, both at the design stage of new lines and at the rearrangement stage of existing lines.**

***Index Terms*—Current phase shift, magnetic-field effects, magnetic fields, power transmission lines.**

I. Introduction

UTILITY recordings derived from the online monitoring of existing transmission lines prove that phase shifts between current phasor terns of some ac double-circuit overhead transmission lines do occur all over their length for most, if not all, of their operating conditions. This happens when the double-circuit line is made of two independent single-circuit lines that connect different nodes of the transmission network but are placed on the same towers for a portion of their length. Such lines commonly carry different amounts of real, reactive, and apparent power under normal operating conditions, according to voltage and frequency regulation constraints [1]. This situation is clearly represented in Fig. 1, where, for an ac double-circuit overhead transmission (ACDOT) line located in Italy, the values of reactive power Q versus real power P, measured hourly at the sending end over one year of operation, are plotted for both circuit I (Q_I versus P_I) and circuit II (Q_{II} versus P_{II}). Fig. 1 highlights that the power flows of the two circuits are mostly not overlapped; hence, they are fairly independent of each other.

In such cases, the ratio among reactive and real power flowing along each of the two circuits can be fairly different from one circuit to the other. As is well known, this ratio is equal to the tangent of the phase-shift angle between the—assumed as symmetrical—rotary systems of phase voltages and currents. Hence, all over the daily service of these ACDOT lines, a significant phase shift can be observed among homologous current phasors of the two circuits; thus, between the whole current terns, as sketched in the current phasor diagram of Fig. 2, where the phase-shift angle between the current terns of the two circuits is indicated as $\Delta\varphi$. This phase shift is referred to as the current phase shift here. It varies with time as the load; it may vary also along the line as the current tern changes with the distance from the sending end.

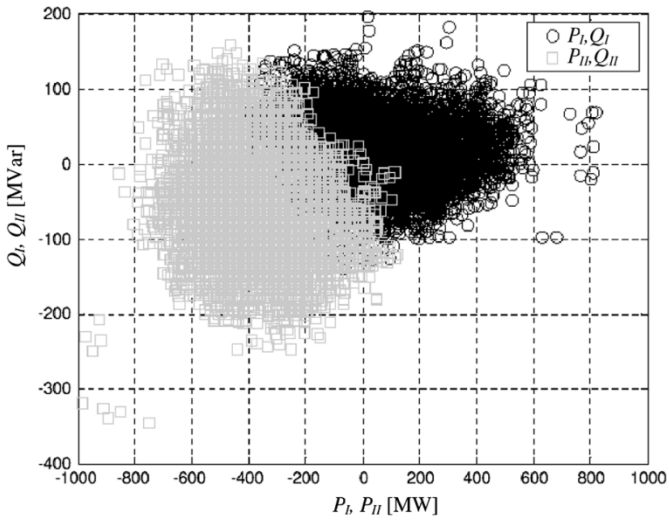

Fig. 1. Reactive versus real power values measured hourly over one year for circuit I (Q_I versus P_I, circles) and circuit II (Q_{II} versus P_{II}, squares) at the sending end of an existing ACDOT line.

As is well known, current phase shifts remarkably affect the magnetic field generated by the ACDOT lines, thus, in turn, the exposure levels of human beings living or working close to them. Neglecting phase-shift effects can involve significant errors in the magnetic-field calculation (up to $\sim$50% and more, as shown concisely in [2] and extensively here), leading to underestimation of the field in some cases, and overestimating it in others. Nevertheless, current phase-shift effects for ACDOT lines are not investigated in several archival literature papers (see, e.g., [3]–[9]) and technical standards (see, e.g., [10]–[12]) about calculation and exposure to magnetic fields generated by power lines. Only a few papers highlight that the phase-shift angle between line currents has a significant influence on the magnetic field established by multiple independent lines [13]–[15].

Manuscript received November 16, 2004; revised March 18, 2005. Paper no. TPWRD-00540-2004.

The author is with the Faculty of Engineering, Department of Electrical Engineering, University of Bologna, Bologna 40136, Italy (e-mail: giovanni.mazzanti@mail.ing.unibo.it).

Digital Object Identifier 10.1109/TPWRD.2005.859273

0885-8977/$20.00 © 2006 IEEE

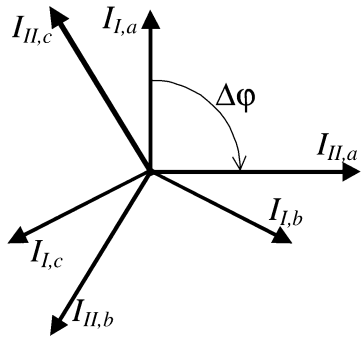

Fig. 2. Phasorial representation of balanced current terns of circuit I and circuit II of an ACDOT line exhibiting a current phase shift.

In the following, the most popular approach to magnetic-field calculation for ac overhead transmission lines is briefly recalled (Section II). Then (Section III), the focus is on ACDOT lines and relevant current phase-shift effects, and the expression of the rms value of magnetic flux density field due to such lines is derived as a function of the phase shift between current terns. Further on (Section IV), this expression is applied to illustrate in detail "static" current phase-shift effects (i.e., the effects relevant to assigned couples of rms current values of the two circuits as a function of the phase-shift angle among current terns), having, as reference cases, the zero phase-shift angle case (current terns in phase) and the 180° phase-shift angle case (current terns in opposition). The correlation is shown between the phase-shift angle and some factors that can either enhance or reduce the magnetic field, such as the arrangement of phase conductors (considering phase in order versus reverse phasing arrangements) and the geometry of the circuits [examining two basic topologies of line towers, and two line sections (i.e., tower section and midspan section)]. The static analysis, repeated for different couples of rms currents, yields a wide variety of magnetic-field profiles and finds out interesting regularities, thus broadening the extent and the significance of the analysis carried out in [2]. The relevant conclusions close Part I of this study and introduce Part II (a forthcoming paper), where the static analysis is converted into a "dynamic" analysis by applying the results of Part I to an existing line and to the relevant load-varying conditions over time periods lasting up to one year.

II. Magnetic-Field Calculation For AC Overhead Transmission Lines

At the power frequency, because of the very large wavelength λ of electromagnetic (EM) fields ($\lambda = 6000$ km at 50 Hz), magnetic-field calculation can be regarded as a quasi-static problem (at least within distances $<\lambda/20$ from the field source [3]) and can be solved by static techniques. Hence, in literature papers, the magnetic field $\boldsymbol{H}$ or magnetic flux density field $\boldsymbol{B}$ (here, bold characters denote vector quantities) from ac overhead power lines is mainly calculated by means of the Biot–Savart law for a linear nonconducting uniform medium [3]–[6], [8], [10]. In the most rigorous approach, both phase conductors and shield wires are considered, together with the catenary shape of line wires, which makes the problem three-dimensional (3-D), requiring numerical solution algorithms (e.g., the finite-element [5] or finite-difference method [7]). The approach is made more complex by eddy currents induced in the ground due to its finite electrical resistivity (accounted for via the image-current approach), as well as in metallic elements close to the line [3].

Dealing with ac overhead transmission lines, the following simplifying assumptions are commonly made, involving, in general, acceptable errors.

1) Electrical resistivity of the soil is assumed as infinite (i.e., image currents induced in the ground are neglected). This holds if the radial distance from the conductor to the field point is much smaller than the ground skin depth $\delta = [\rho_g/(\pi\mu_0 f)]^{0.5}$, where ρ_g is the ground resistivity, μ_0 is the magnetic permeability of free space, and f is frequency [3]. At $f = 50$ Hz, δ ranges from 225 to 2250 m, for ρ_g from 10 to 1000 Ωm (typical values). In [4], it is shown that for such values of ρ_g and for a typical overhead transmission line, errors involved by assuming infinite ground resistivity are $<1\%$ at 100 m from a line axis. Therefore, such a hypothesis holds for points within or close to the right of way, those most critical from the viewpoint of human exposure.
2) The effect of phase current unbalance is neglected; thus, only symmetric terns of phase currents are considered for magnetic-field calculation [5]. Indeed, commonly phase current unbalance is remarkable for distribution systems, but low for transmission lines. In [4], it is shown that, for a typical overhead transmission line, negative- and zero-sequence currents are a few percent of positive-sequence currents.
3) Currents induced in conductive elements within the soil or close to the line (e.g., tower structures, counterpoise wires, metallic fences, irrigation pipes, other power/communication lines, and so on) are ignored. Hence, the only field sources examined are phase conductors, since return currents in the shield wires can be neglected thanks to the previous hypotheses 1 to 3.
4) The effect of harmonic currents that can be significant in medium-voltage (MV) and low-voltage (LV) distribution systems is neglected [4], [5].
5) Phase conductors and shield wires are straight, horizontal, and infinitely long. Then (and by virtue of approximation 3), the magnetic-field problem becomes two-dimensional (2-D) [i.e., vectors $\boldsymbol{H}$ and $\boldsymbol{B}$ at a field point $\boldsymbol{x}$ lie in a plane perpendicular to line axis (let's call this plane line section) and can be calculated assuming the ground clearance for the whole line as equal to the actual line clearance at the line section of interest]. This involves moderate errors over line sections along the line; errors are highest at the tower section, lowest and typically below 1% at midspan, where the magnetic field is highest [4], [16]. However, errors due to assumption 5 are among the most significant ones caused by hypotheses 1–5.

If assumptions 1–5 hold, the Biot–Savart law is equivalent to Ampere's law applied at a given line section, namely [8], [10]

$$\hat{\boldsymbol{B}}(\boldsymbol{x}_j) = \frac{\mu_0}{2\pi}\sum_{i=1}^{M}\frac{\hat{I}_i}{d_{i,j}}\boldsymbol{u}_i \times \boldsymbol{u}_{i,j} \tag{1}$$

where $\hat{\boldsymbol{B}}\ (\boldsymbol{x}_j)$ is the magnetic flux density field at $\boldsymbol{x}_j$ ($j = 1,\ldots,N, N$ being the number of selected points where the field should be calculated at the line section of interest), $\hat{I}_i$ is the ith current phasor ($i = 1,\ldots,M, M$ is the number of phase conductors; and a $\wedge$ over a variable indicates that it is a phasor quantity), $d_{i,j}$ is the distance from the ith phase conductor to the jth field point, $\boldsymbol{u}_i$ and $\boldsymbol{u}_{i,j}$ are unit vectors in the direction of the ith conductor and of $d_{i,j}$, respectively. Note that $M = 3$ for single-circuit lines, and $M = 6$ for double-circuit lines.

By setting a 2-D Cartesian coordinate system orthogonal to the line axis, (1) can be written in terms of $\hat{B}_x$, $(\boldsymbol{x}_j)$, and $\hat{B}_y$ $(\boldsymbol{x}_j), x$ and y components of $\hat{\boldsymbol{B}}(\boldsymbol{x}_j)$ [10]

$$\hat{B}_x(\boldsymbol{x}_j) = \frac{\mu_0}{2\pi}\sum_{i=1}^{M}\hat{I}_i\frac{(y_i - y_j)}{(x_i - x_j)^2 + (y_i - y_j)^2} \tag{2}$$

$$\hat{B}_y(\boldsymbol{x}_j) = \frac{\mu_0}{2\pi}\sum_{i=1}^{M}\hat{I}_i\frac{(x_j - x_i)}{(x_i - x_j)^2 + (y_i - y_j)^2}. \tag{3}$$

III. AC Double-Circuit Overhead Transmission Lines and Current Phase-Shift Effects

The rms value of magnetic flux density strength at a given location $B\ (\boldsymbol{x}_j)$ is of main interest from the viewpoint of human exposure to low-frequency electromagnetic fields [10]–[12]. Therefore, it is worthwhile deriving explicitly from (2) and (3), the rms value of magnetic flux density for the ACDOT lines, also because by doing so, the effect of current phase shifts for such lines can be better highlighted. In order to achieve this goal, the phasor notation should be replaced with the instant-value notation, as follows [2]. Under the previous assumption of symmetric voltage and current terns for both circuits, one phase voltage of the first circuit is chosen as the phase reference and the phase-shift angles among reference phase voltage and current terns of the first (I) and second (II) circuit are defined as φ_I and φ_{II}, respectively, thereby defining the phase-shift angle between the two current terns of the two circuits $\Delta\varphi$

$$\Delta\varphi = \varphi_{II} - \varphi_I. \tag{4}$$

Thus, $\Delta\varphi > 0$[1] if the current tern of circuit II is lagging that of circuit I (Fig. 2); hence, the instant value of the ith phase current of the ACDOT line can be written as [2]

$$I_i(t) = \sqrt{2}I_i\sin[\omega t - \Delta_i - 2(i-1)\pi/3], \quad i = 1,\ldots,6 \tag{5}$$

where $\omega = 2\pi f$ is the angular frequency, I_i is the rms value of the ith phase current, and Δ_i is a quantity such that it holds:

1) $I_i = I_I, \Delta_i = 0$ for $i = 1, 2, 3$ (i.e., for phase currents of circuit I);
2) $I_i = I_{II}, \Delta_i = \Delta\varphi$ for $i = 4, 5, 6$ (i.e., for currents of circuit II).

By replacing current phasors in (2) and (3) with instant values of phase currents, as expressed by (5), the following instant-value relationships are obtained:

$$B_x(\boldsymbol{x}_j, t) = \frac{\mu_0}{\pi\sqrt{2}}\sum_{i=1}^{6}\left\{\frac{I_i\sin\left[\omega t - \Delta_i - 2(i-1)\frac{\pi}{3}\right](y_i - y_j)}{(x_i - x_j)^2 + (y_i - y_j)^2}\right\} \tag{6}$$

$$B_y(\boldsymbol{x}_j, t) = \frac{\mu_0}{\pi\sqrt{2}}\sum_{i=1}^{6}\left\{\frac{I_i\sin\left[\omega t - \Delta_i - 2(i-1)\frac{\pi}{3}\right](x_j - x_i)}{(x_i - x_j)^2 + (y_i - y_j)^2}\right\}. \tag{7}$$

Finally, $B(\boldsymbol{x}_j)$ can be derived by calculating from (6) and (7) the rms values of $B_x(\boldsymbol{x}_j, t), B_y(\boldsymbol{x}_j, t)$ (i.e., $B_x(\boldsymbol{x}_j), B_y(\boldsymbol{x}_j)$), respectively

$$B(\boldsymbol{x}_j) = \sqrt{[B_x(\boldsymbol{x}_j)]^2 + [B_y(\boldsymbol{x}_j)]^2}. \tag{8}$$

From (6)–(8), it is clear that also the value of Δ_i (thus, the value of $\Delta\varphi$) determines the rms value of magnetic flux density strength $B(\boldsymbol{x}_j)$ (referred to for the sake of brevity as B-field from now on; see also [17]); thus, the human exposure at a field point. In order to evaluate quantitatively the current phase-shift effect for ACDOT lines, a simple code-named BDP after B-field double-circuit phase shift has been developed in the MATLAB environment. The BDP code, which actually does not present new elements with respect to previous codes, apart from the focus on phase-shift effects and the ability of analyzing multiple load conditions in sequence, is based on relationships (6)–(8) and is implemented in two versions.

1) The "static" BDP code, presented in [2] and used in Part I of this investigation, calculates the B-field established by an ACDOT line for a single constant load condition, at N field points located all at the same height from the ground in the part of the line section where above assumptions 1–5 hold.[2]
2) The "dynamic" BDP code repeats the same calculation of the static code over a number K of different load-varying conditions, for a time period lasting up to one year or more.

Both versions of the BDP code have the same geometric input quantities (i.e., coordinates $\{x_i, y_i\}$ of phase conductors ($i = 1,\ldots,6$) and $\{x_j, y_j\}$ of field points ($i = 1,\ldots,N$)). In addition, the static BDP code requires rms values and phases of phase currents of the two circuits at the chosen time instant (or load condition), while the dynamic BDP code needs these values at all of the K different time instants (or load conditions) over the selected time period to be analyzed in the time-dependent calculations (see Part II of this study for further details).

The BDP code was validated [2] with a reliable reference program, the CAMPI code (developed in C^{++} language by IFAC-CNR, an Italian public research institute, and validated, in turn,

[1]Apart when focusing on periodicity features (e.g., between $\Delta\varphi$ and $2\pi - \Delta\varphi$), $\Delta\varphi$ is expressed here in electrical degrees, and as ranging from $-180°$ to 180°, or (more frequently, for practical reasons) from 0° to 360°.

[2]As argued from the discussion at Section II, hypotheses 1–5 are commonly matched within a part of the line section centered on the line axis and of width 200 m along the x-axis, where all field points chosen here are located.

by means of other codes and field measurements [18]), that performs "static" electric- and magnetic-field calculations at power frequency for different conductor geometries. The comparison was fully satisfactory, with differences between the results given by the two codes always far lower than 0.1%. Some of the validation results are shown in the following sections.

IV. Static Analysis of Current Phase-Shift Effects

A. Guidelines for the Static Analysis

As anticipated in Section III, the static BDP code is used here for a detailed computational analysis of "static" current phase-shift effects on the magnetic field established by ACDOT lines. The static analysis consists of calculations relevant to assigned load conditions, performed for given and constant rms current values of the two circuits and letting the phase-shift angle span over the range [0°; 360°], corresponding to different possible relative amounts and/or flow directions of real and reactive power on each circuit, for the same amount of circuit apparent power. By this way, a wide variety of field profiles at a given line section is obtained, that differ remarkably from those relevant to the two reference cases often considered as the only possible [i.e., $\Delta\varphi$ = 0°= 360° (currents "in the same direction") and $\Delta\varphi = 180°$ (currents "in opposite direction")]. The analysis is then repeated for different couples of rms current values, thereby finding interesting general features of field profiles that do not depend on the current values, but only on $\Delta\varphi$, thus emphasizing the role played by the current phase shift on the magnetic fields from ACDOT lines. This analysis is meaningful since, as can be argued from Fig. 1 and as shown widely in Part II of this study, for some existing ACDOT lines, the current phase-shift angle is intermediate between the 0° case and the 180° case for most operating conditions of the lines. In those situations, the static analysis is essential for a better understanding of the time evolution of the magnetic field established by such ACDOT lines as load conditions change over the year; thus, for a thorough evaluation of yearly mean/median field levels representative of human exposure to magnetic fields generated by the lines.

For a better illustration of the effects of line geometry and conductor arrangement, and for broadening the validity of the static analysis with respect to the concise treatment performed in [2], two typical Italian 380-kV ACDOT lines are examined here, each one characterized by the relevant towers (thus, by the corresponding peculiar geometry of phase conductors), namely the so-called MV tower and NV tower. The two different conductor geometries at the MV tower section and at the NV tower section, respectively, are sketched in Figs. 3 and 4, where single circuits I and II, conductor heights above ground h, and horizontal distances d are shown. The figures also illustrate two alternative vertical arrangements of homologous phase conductors[3] of the two circuits, that is, phase in order (in which the homologous phases are at the same height), and reverse phasing, also

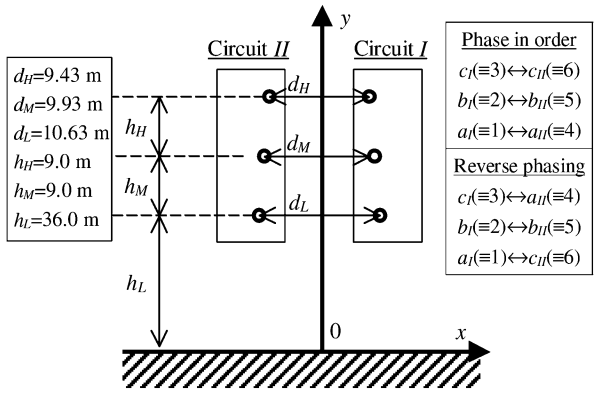

Fig. 3. Sketch (not in scale) of the conductor geometry of a typical Italian 380-kV ACDOT line, the so-called MV tower line, at the tower section. Two possible vertical arrangements of phase conductors (phase in order and reverse phasing) are also shown.

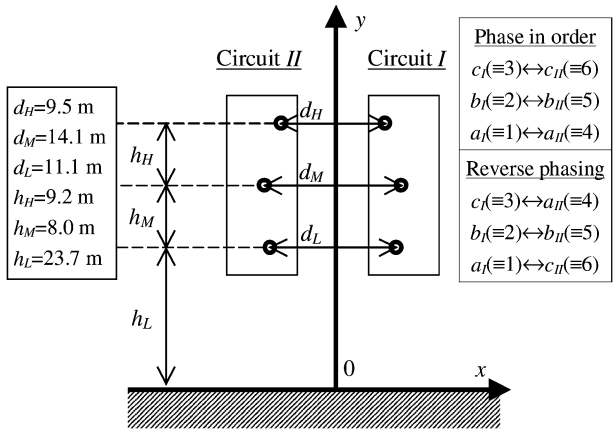

Fig. 4. Same as Fig. 3, but with reference to the so-called NV tower.

referred to as "low-reactance" [14]. The low-reactance arrangement always mitigates the electric field, and sometimes also the B-field, depending on current phase shift, as shown widely in the following.

Of course, magnetic-field profiles will reach their lowest values at the tower section, and their highest values at the midspan section. Thus, in B-field calculations, for both kinds of 380-kV ACDOT lines, only the tower section and midspan section will be considered as yielding "extreme" B-field profiles. It must be pointed out that, for a same tower topology, tower height and span length can vary depending on the line route; conductor heights above ground level are affected accordingly. Hence, the cases considered here should be retained as reference cases for the calculation of the magnetic field generated by ACDOT lines, and for the analysis of the relevant current phase-shift effects. However, results similar to those illustrated in the following can be obtained also for different conductor heights at both midspan and/or tower sections as well as for different towers.

Many calculations were performed by the author in order to analyze "static" current phase-shift effects on the magnetic field established by ACDOT lines. A brief synthesis of them, aimed

[3]Homologous phases are 1 versus 4, 2 versus 5, 3 versus 6, according to (1)–(8), or a_I versus a_{II}, b_i versus b_{II}, c_i versus c_{II}, according to a more common notation [1].

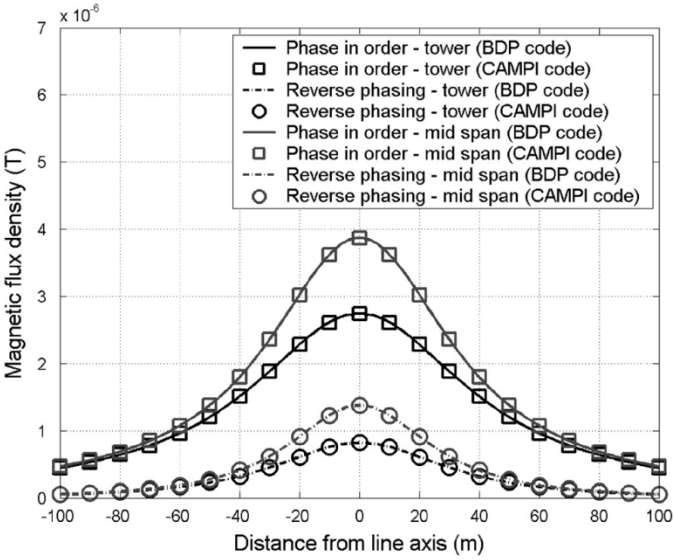

Fig. 5. B-field values calculated by the BDP code (lines) and the CAMPI code (symbols) for $\Delta\varphi = 0°$ at some points 1 m above ground level for the MV tower line, at tower section ($h_L = 36$ m, black objects) and at midspan section ($h_L = 29$ m, gray objects), for both the phase in order (solid lines + squares) and the reverse phasing (dashed–dotted lines + circles) conductor arrangement. $I_I = I_{II} = 855$ A.

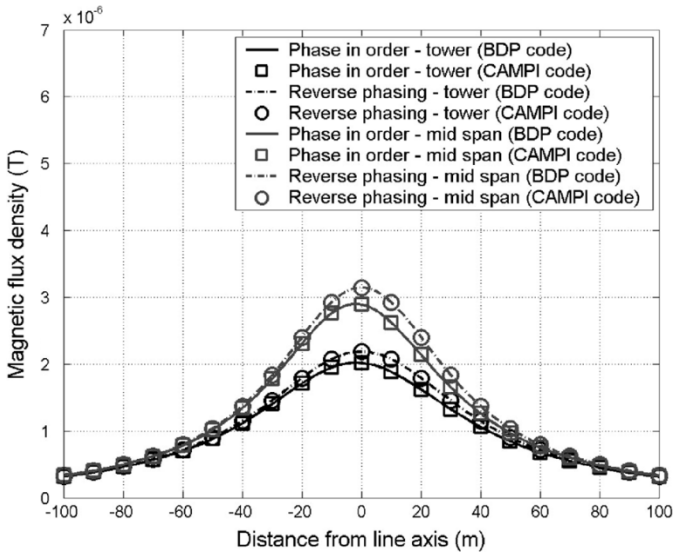

Fig. 6. Same as Fig. 5, but for $\Delta\varphi = 90°$.

at highlighting the most interesting cases and the relevant important observations to be made, is shown here below.

B. Static Analysis for the MV Tower Line

Let us consider the MV tower line first (Fig. 3). Fig. 5 displays the B-field values calculated by the BDP code (lines) and the CAMPI code (symbols) under the assumption that $\Delta\varphi = 0°$ (i.e., no phase shift among current terns of the two circuits) at some points 1 m above the ground level in correspondence of the MV tower section (black objects in the figure; $h_L = 36$ m), and of the midspan section (gray objects in the figure; a fairly high value for h_L at the midspan section is taken (i.e., 29 m), relevant to an existing line examined in [2]) for both the phase in order (solid lines and squares) and the reverse phasing (dashed–dotted lines and circles) conductor arrangement (see also the figure legend for a better understanding). For these calculations, a value of 855 A has been selected for rms phase currents of both single-circuit lines, which incidentally coincides with the current at the sending end of a 100-km-long 380-kV (at the receiving end) single-circuit line, carrying its natural load and having the following conductor formation: triple aluminum-conductor steel-reinforced bundle, with 3×585 mm^2 total cross-section [19]. In fact, if the ACDOT line is made up of two independent single-circuit lines, the case $I_I = I_{II}$ to be considered is rather uncommon, but serves here as a reference example from which the analysis can be started, as well as a prototypical validation case for the BDP code.

Fig. 6 reports B-field values calculated by the BDP code (lines) and the CAMPI code (symbols) at the same field points and under the same assumptions of Fig. 5, except that $\Delta\varphi = 90°$ (current terns in quadrature) is assumed. As Figs. 5 and 6 show, the agreement between the two codes is very satisfactory both in the $\Delta\varphi = 0°$ and in the $\Delta\varphi = 90°$ case, both for the phase in order and for the reverse phasing arrangement, both at tower and at midspan section; indeed, the symbols (CAMPI code results at 21 equally spaced field points at various distances from line axis) are practically overlapped to the lines (BDP code results at 201 equally spaced points at various distances from line axis). This supports the results of the BDP code.

The analysis and the comparison between Figs. 5 and 6 enable three main preliminary observations to be made on the "static" effects of current phase shift on the magnetic field generated by ACDOT lines, namely the following.

a) B-field values computed setting $\Delta\varphi = 0°$ (Fig. 5) are very different from those derived taking $\Delta\varphi = 90°$ (Fig. 6), for both phase arrangements and at both line sections; hence, accounting for a current phase shift is fundamental for a correct calculation of the B-field from ACDOT lines made of independent single circuits that may exhibit even higher values of $\Delta\varphi$ [2].

b) Phase arrangement is essential to determine the field profile at a line section. As is also intuitive (see Figs. 3 and 4), for $\Delta\varphi = 0$ (Fig. 5) the reverse phasing arrangement provides much lower B-field values than the phase in order one, both at tower and at midspan section; this situation reverses for $\Delta\varphi = 180°$ (omitted here for the sake of brevity), when the phase in order arrangement is to be preferred to the reverse phasing one from the viewpoint of field mitigation.

c) The transition in convenience between reverse phasing and phase in order takes place at a value of $\Delta\varphi$ slightly lower than 90°, since at $\Delta\varphi = 90°$ the B-field profile generated by the reverse phasing arrangement has already exceeded completely that due to the phase in order one, both at the tower and at midspan section (Fig. 6), and since in the [0°, 180°] interval, the reverse phasing field profile is a monotonically increasing function of $\Delta\varphi$, while the phase in order field profile is a monotonically decreasing function of $\Delta\varphi$, as shown below.

d) The difference between field profiles at the tower and midspan section, for a given conductor arrangement and

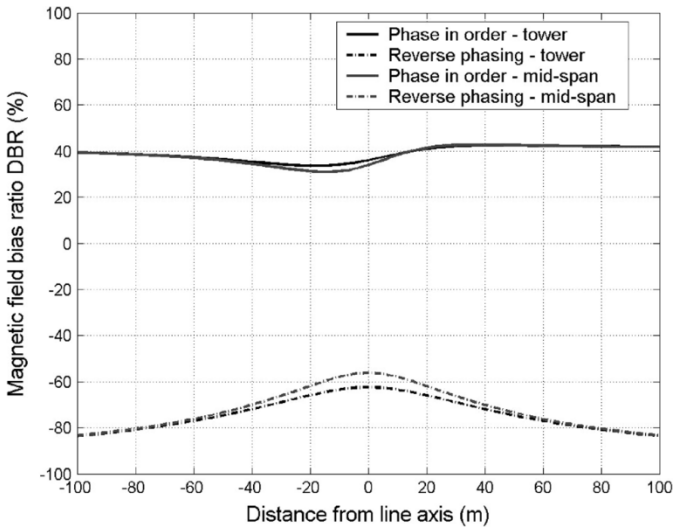

Fig. 7. Magnetic field bias ratio ΔB_R from BDP code calculations for phase in order (solid lines) and reverse phasing (dash-dot lines) arrangements and for the tower section (black lines) and the midspan section (gray lines) at the same points of Figs. 5 and 6.

$\Delta\varphi$ value, is very small at distances far from the line axis, where the phase-shift angle and conductor arrangement have a stronger effect than the conductor height, at least for the values of h_L examined up to now.

For further emphasizing the "static" effects of the current phase shift on magnetic field from ACDOT lines and, in particular, the errors made when neglecting such a phase-shift, the percent magnetic-field bias ratio ΔB_R can be defined, that is

$$\Delta B_R = 100[B(\Delta\varphi = 0) - B(\Delta\varphi)]/B(\Delta\varphi) \qquad (9)$$

where $B(\Delta\varphi = 0)$ is the value of the B-field calculated neglecting the "actual" value of the phase-shift angle $\Delta\varphi$ (i.e., taking $\Delta\varphi = 0$), while $B(\Delta\varphi)$ is the value of the B-field obtained considering such a value. Equation (9) implies that neglecting the actual value of $\Delta\varphi$ involves an overestimation of the B-field generated by the ACDOT line if $\Delta B_R > 0$, an underestimation if $\Delta B_R < 0$.

The values of ΔB_R computed from the BDP-code profiles reported in Figs. 5 and 6 are displayed in Fig. 7 for both the phase in order (solid lines) and the reverse phasing (dashed–dotted lines) arrangement and for both the tower section (black lines) and the midspan section (gray lines); note that the values of $B(\Delta\varphi = 0)$ are attained from Fig. 5, while the values of $B(\Delta\varphi = 90°)$ are derived from Fig. 6. Fig. 7 shows that for the selected tower structure, field points and current values neglecting a "real" $\Delta\varphi = 90°$ involve an overestimation of the field that ranges from 30% to 42% in the phase in order case, an underestimation of the field (much worse from the viewpoint of human exposure) that ranges from 55% to 85% in the reverse phasing case. Note that, for a given conductor arrangement, errors are almost the same at the two considered line sections; since these sections yield extreme values of a magnetic field, it can be argued that percent errors are almost constant all over the line length, at least under the approximations made in Section II and for the chosen conductor heights. It can also be argued that, at a given line section, the largest percent errors made by neglecting current phase shift occur outside the right of way, where residential buildings can be placed; thus, such errors can affect significantly the evaluation of human exposure.

In addition, a careful analysis of Figs. 5–7 offers the following suggestions.

i) In the case of reverse phasing arrangement, B-field profiles are symmetric with respect to the line axis both for $\Delta\varphi = 0$ and for $\Delta\varphi = 90°$ and both at the tower and midspan section.
ii) In the case of phase in order arrangement, B-field profiles are symmetric with respect to the line axis for $\Delta\varphi = 0$, while they are asymmetric when $\Delta\varphi = 90°$, both at the tower and midspan section (see the following for further details).

A thorough "static" analysis for the MV tower line requires that the whole range of actual load conditions be investigated, while previous calculations are restricted to fixed and equal currents in the two circuits, and to only two values of $\Delta\varphi$. As proved by measurements performed during line operation [2], load conditions of existing ACDOT lines with independent single circuits feature a very wide range of different amounts of real and reactive power; hence, a wide variety of couples of unequal rms phase currents in the two circuits as well as of values of the phase-shift angle $\Delta\varphi$, the latter ranging over the whole interval from 0° to 360°. Therefore, in principle, a large number of combinations of $\Delta\varphi$ values and couples of single-circuit rms currents should be considered for a rigorous and exhaustive "static" analysis.

On the other hand, it can be argued that rms currents are time constants in the static calculation, and can be properly factored out in (6)–(8). Moreover, often one of the two circuits, say circuit I, carries less current than the other; hence, its current I_I can be expressed in the per-unit value of the other current I_{II} (i.e., $I_I = pI_{II}$), where p is the ratio I_I over I_{II} (note that, for example, Figs. 5–7 are all relevant to a value of $p = 1$). Then, according to (6)–(8), the rms magnetic flux density values for a given line and at a given line section can be calculated as a function of $\Delta\varphi$ for a unit value of I_{II} and for several values of p ranging from 1 to 0, thereby accounting for a more and more uneven ratio among homologous phase currents of the two circuits. A series of B-field profiles calculated as a function of $\Delta\varphi$ for a given value of p and for a unit value of reference current I_{II} can be expressed in Tesla over Ampere and have general validity for every couple of values of I_I and I_{II} such that $I_I = pI_{II}$; such a "family" of magnetic-field profiles will be referred to from now on as per-unit-current (p.u.c.) profiles. Indeed, the B-field profiles at a given line section for a particular couple of currents can be derived from the relevant p.u.c. profiles (i.e., those featuring a value of p equal to the ratio I_I/I_{II} of that particular couple) by simply multiplying the B-field values of these p.u.c. profiles by the particular (actual) value of reference current I_{II}. For this reason, only p.u.c. profiles are shown from now on.

Figs. 8 and 9 show B-field p.u.c. profiles calculated by the static BDP code at the midspan section of an MV tower line for several values of $\Delta\varphi$ over the interval 0°–360° (i.e., 0° = 360°,

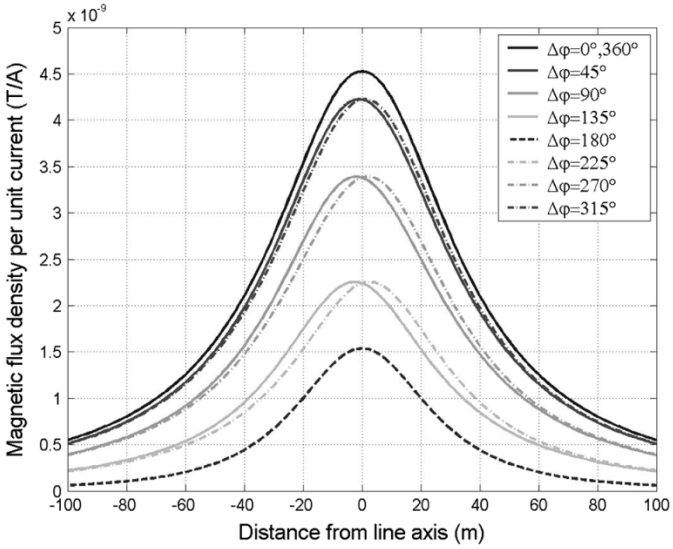

Fig. 8. B-field p.u.c. profiles obtained by the BDP code for several values of $\Delta\varphi \in [0°, 360°]$ (see legend) at some points 1 m above ground level for the MV tower line at the midspan section ($h_L = 29$ m), for the phase in order arrangement $I_I = 100\% I_{II} (p = 1.0)$.

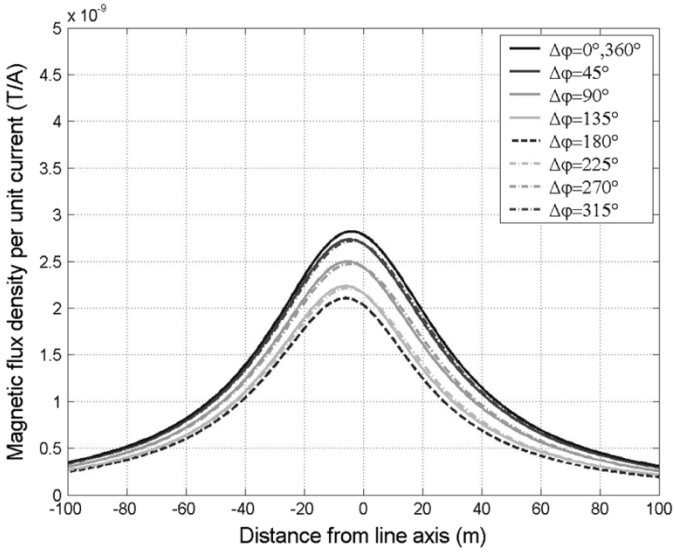

Fig. 9. Same as Fig. 8, but for $I_I = 20\% I_{II} (p = 0.2)$.

45°, 90°, 135°, 180°, 225°, 270°, 315°) for the phase-in-order conductor arrangement. Fig. 8 is relevant to $p = 1.0$, Fig. 9 to $p = 0.2$; lower values of p are not considered, both for the sake of brevity and because for such p values, current I_{II} is so predominant that it hides, in practice, phase-shift effects.

Dealing with Fig. 8, it provides a first example of derivation of a particular B-field profile from the corresponding p.u.c. profile. Indeed, the curve relevant to $\Delta\varphi = 0°$ corresponds to the phase in order midspan curve of Fig. 5 (gray solid line), exhibiting a value of $p = 1$ as well ($I_I = I_{II} = 855$ A); in fact, the maximum of $4.53 \cdot 10^{-9}$ T/A of the $\Delta\varphi = 0°$ curve in Fig. 8, multiplied by 855 A, equals the maximum of $3.87 \cdot 10^{-6}$ T of the phase in order midspan curve in Fig. 5; the same holds for all other 201 field points that compose the field profile of the two homologous curves. Likewise, the curve relevant to $\Delta\varphi = 90°$ in Fig. 8 corresponds to the phase in order midspan curve of Fig. 6 (gray solid line), exhibiting a value of $p = 1$, too ($I_I = I_{II} = 855$ A); in fact, the maximum of $3.39 \cdot 10^{-9}$ T/A of the $\Delta\varphi = 90°$ curve in Fig. 8, multiplied by 855 A, equals the maximum of $2.90 \cdot 10^{-6}$ T of the phase in order midspan curve in Fig. 6.

Fig. 8 also confirms the following for the phase-in-order arrangement.

1.1) B-field profiles decrease with $\Delta\varphi$ in the [0°, 180°] interval, reaching their minimum at $\Delta\varphi = 180°$, then increase in the [180°, 360°] interval, up to their maximum at $\Delta\varphi = 360° = 0°$.

1.2) B-field profiles at the midspan section are asymmetric with respect to the line axis, with the exception of $\Delta\varphi = 0°$ and $\Delta\varphi = 180°$ profiles; more precisely, Fig. 8 shows that for $p = 1$, the profiles obtained for $\Delta\varphi$ and for $2\pi - \Delta\varphi$ are specularly symmetric to each other with respect to the line axis.

Passing from Fig. 8 to Fig. 9, as p decreases from 1.0 to 0.2 (i.e., as I_{II} predominates over I_I, becoming the most relevant source of magnetic field), the following comments can be made.

1.3) Field profiles enhance their asymmetry with respect to the line axis, displacing themselves toward the negative-x half-plane, where circuit II lies (Fig. 3).

1.4) The specular symmetry between $\Delta\varphi$ and $2\pi - \Delta\varphi$ profiles observed for $p = 1$ is lost, but they are still different from each other, even if such differences are rather small far from line axis. This proves that subintervals [0°, 180°] and [180°, 360°] yield different field profiles, and support the need of a careful analysis over the whole range of variation of $\Delta\varphi$.

1.5) Field profiles become much less sensitive to $\Delta\varphi$ values, tending to be fairly similar to each other over the whole range of variation of $\Delta\varphi$.

1.6) For $\Delta\varphi = 0°$, the magnetic field decreases all over the line section, particularly close to line axis; for $\Delta\varphi = 180°$, the magnetic field increases all over the line section, particularly far from the line; for intermediate values of $\Delta\varphi$, an intermediate behavior is observed. On the whole, as p decreases, the situations in which field decreases are the majority, even if some non-negligible increases are observed, particularly far from line axis, where residential buildings can be placed and humans may live.

Statement 1.6 is an interesting consequence of Statement 1.5, and deserves more comments. Indeed, as current in circuit I is reduced from 100% to 20% of the current in circuit II, the decrease in sensitivity of field profiles to phase-shift angle involves that the reduction of magnetic field at a given line section is not uniform over the range of variation of $\Delta\varphi$ and at the various distances from the line axis, so that the field even increases in some cases, for some values of $\Delta\varphi$ and/or at some distances from the line axis. Indeed, for the value of $\Delta\varphi$ that is most effective in enhancing the field for the phase in order arrangement (i.e., 0°, the value at which the source contributions from both circuits add most effectively to each other, see Fig. 5), a significant magnetic field decrease is observed all over the line section as p decreases, since one of the two field sources is weakened;

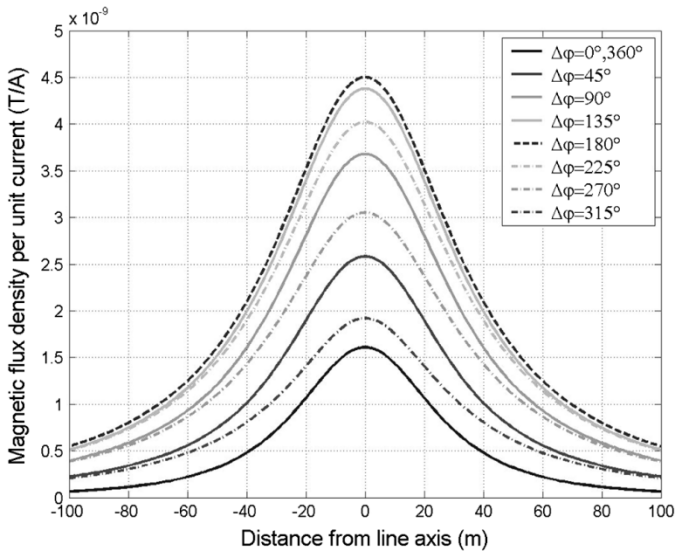

Fig. 10. B-field p.u.c. profiles obtained by the BDP code for several values of $\Delta\varphi \in [0°, 360°]$ (see legend) at some points 1 m above ground level for the MV tower line at midspan section ($h_L = 29$ m), for the reverse phasing arrangement. $I_I = 100\% I_{II} (p = 1.0)$.

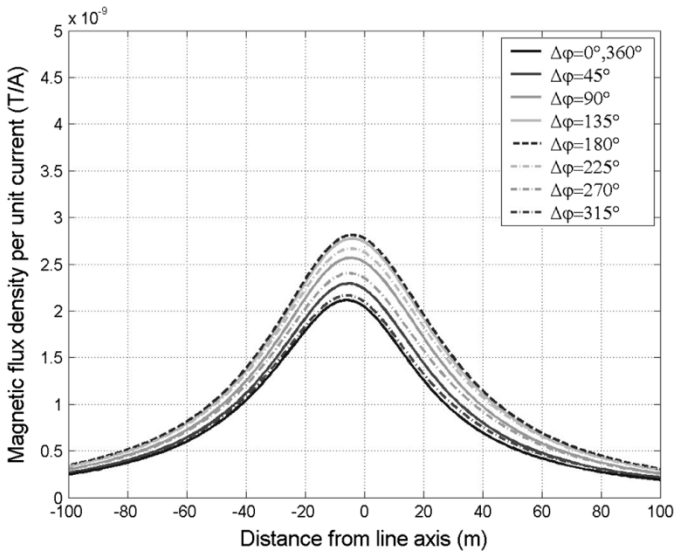

Fig. 11. same as Fig. 10, but for $I_I = 20\% I_{II} (p = 0.2)$.

the decrease, both in absolute and in percent value, is particularly remarkable close to the line axis. On the contrary, for the value of $\Delta\varphi$ that is most effective in reducing the field for the phase in order arrangement (i.e., 180°, the value at which the source contributions from both circuits cancel most effectively with each other), a significant field increase is observed all over the line section as p decreases; the increase in percent value is particularly remarkably far from the line.

Passing to the reverse phasing arrangement, Figs. 10 and 11 show, for such an arrangement, B-field p.u.c. profiles calculated by the static BDP code at the midspan section of an MV tower line for the values of $\Delta\varphi \in [0°, 360°]$ already considered in Figs. 8 and 9; Fig. 10 is relevant to $p = 1$, Fig. 11 to $p = 0.2$.

Analogously to Fig. 8, it can be argued that the curve relevant to $\Delta\varphi = 0°$ in Fig. 10 corresponds to the reverse phasing midspan curve of Fig. 5 (gray dashed–dotted line), that exhibits a value of $p = 1$ as well ($I_I = I_{II} = 855$ A); in fact, the maximum of $1.61 \cdot 10^{-9}$ T/A of the $\Delta\varphi = 0°$ curve in Fig. 10, multiplied by 855 A, equals the maximum of $1.38 \cdot 10^{-6}$ T of the reverse phasing midspan curve in Fig. 5; the same holds for all of the other 201 field points that compose the field profile of the two homologous curves. Likewise, in Fig. 10, the curve relevant to $\Delta\varphi = 90°$ corresponds to the reverse phasing midspan curve of Fig. 6 (gray dashed–dotted line), that exhibits a value of $p = 1$, too ($I_I = I_{II} = 855$ A also in this case); in fact, the maximum of $3.68 \cdot 10^{-9}$ T/A of the $\Delta\varphi = 90°$ curve in Fig. 10, multiplied by 855 A, equals the maximum of $3.15 \cdot 10^{-6}$ T of the reverse phasing midspan curve in Fig. 6.

Fig. 10 also confirms that for the reverse phasing arrangement.

2.1) B-field profiles increase with $\Delta\varphi$ in the [0°, 180°] interval, up to their maximum at $\Delta\varphi = 180°$, then decrease in the [180°, 360°] interval, down to their minimum at $\Delta\varphi = 360° = 0°$.[4]

2.2) B-field profiles at the midspan section are symmetric with respect to the line axis, but $\Delta\varphi$ and $2\pi - \Delta\varphi$ profiles are different from each other.

Passing from Fig. 10 to Fig. 11 as p decreases from 1.0 to 0.2 (i.e., as I_{II} predominates over I_I) it can be seen that:

2.3) Field profiles become asymmetric with respect to the line axis, displacing themselves towards the negative-x half-plane.

2.4) $\Delta\varphi$ and $2\pi - \Delta\varphi$ profiles are still different from each other, even if such differences are rather small at distances far from the line axis. This proves the diversity of subinterval [0°, 180°] from subinterval [180°, 360°] from the viewpoint of the field profiles.

2.5) Field profiles become much less sensitive to $\Delta\varphi$ values, tending to be fairly similar to each other over the whole range of variation of $\Delta\varphi$.

2.6) For $\Delta\varphi = 180°$, the magnetic field decreases all over the line section, particularly close to the line axis; for $\Delta\varphi = 0°$, the magnetic field increases all over the line section, particularly far from the line. For intermediate values of $\Delta\varphi$, intermediate behavior is observed. On the whole, as p decreases, the field decreases mostly as well, even if some non-negligible increases are observed, particularly far from the line axis.

Once more, the last statement is an interesting consequence of the decrease in sensitivity of field profiles to phase-shift angle, involving that as the current in circuit I is reduced from 100% to 20% of the current in circuit II, the reduction of the magnetic field at a line section is not uniform over the range of variation of $\Delta\varphi$ and at the various distances from line axis, so

[4]This holds for the $\Delta\varphi$ values in the graphs; a deeper analysis reveals that between 153° and 204°, as well as between 333° and 24°, p.u.c. profiles are practically overlapped, some of them being slightly higher close to line axis, some others far from the line axis. This further analysis, omitted here for the sake of brevity, confirms that some current phase-shift effects are not intuitive.

that the field even increases, in some cases, for some values of $\Delta\varphi$ and/or at some distances from the line axis. Indeed, for $\Delta\varphi = 180°$ (the most effective value in enhancing the field for the reverse phasing arrangement), a significant magnetic field decrease is observed all over the line section as p decreases; the decrease, both in absolute and in percent value, is, in particular, remarkable at distances close to the line axis. On the contrary, for $\Delta\varphi = 0°$ [the most effective value in reducing the field for the reverse phasing arrangement (Fig. 5)], a significant field increase is observed all over the line section; the percent value increase is, in particular, remarkable at distances far from the line; thus, where humans may live.

All of the considerations made when discussing Figs. 8–11, relevant to the midspan section, also hold for the tower section. On the whole, they emphasize the role played by the current phase shift on magnetic fields generated by ACDOT lines, and its importance from the viewpoint of human exposure to such fields. It is also interesting to point out that phase-shift effects are sometimes intuitive, sometimes hidden and nontrivial, and can be revealed only by a careful and detailed analysis.

One more interesting and nonintuitive effect of $\Delta\varphi$ on the magnetic field from ACDOT lines is the way in which the transition in convenience (from the viewpoint of human exposure to magnetic fields) between reverse phasing and phase in order over subinterval [0°, 180°] takes place, as well as the opposite transition in convenience between phase in order and reverse phasing over subinterval [180°, 360°]. As mentioned above, the former transition means that at a given field point in a selected line section, the rms magnetic flux density value obtained by the phase in order conductor arrangement, say $B_{\rm ph}$, becomes lower than the rms magnetic flux density value obtained by the reverse phasing conductor arrangement, say $B_{\rm rev}$, at a value of $\Delta\varphi \sim 90°$. Actually, a careful analysis of p.u.c. profiles calculated for $\Delta\varphi \in [0°, 180°]$ at the midspan section shows that such a transition occurs at a progressively increasing number of field points as $\Delta\varphi$ rises from 82° to 90°; at $\Delta\varphi = 90°$, the transition is complete (i.e., $B_{\rm ph} < B_{\rm rev}$) all over the section. Let us call $\Delta\varphi'$ the values of $\Delta\varphi \in [82°, 90°]$ for which this transition takes place.

What is neither obvious nor intuitive is that the field points [identified each by the relevant distance from line axis (i.e., by the relevant coordinate $x_j, j = 1, \ldots, N; y_j = 1$ m, since they are all located at the same height above the soil)] at which, at a given value of $\Delta\varphi'$, the transition has already occurred (i.e., at which $B_{\rm ph}(x_j, \Delta\varphi') < B_{\rm rev}(x_j, \Delta\varphi')$) do not depend on the particular couple of rms phase current values in the two circuits I_I and I_{II}, thus ultimately they do not depend on I_{II} and p. In other words, the extremes of the range where the transition has already occurred for a given $\Delta\varphi'$ [i.e., the minimum value of coordinate x_j (let us call it x_L) and the maximum value of coordinate x_j (let us call it x_U) at which $B_{\rm ph}(x_j, \Delta\varphi') < B_{\rm rev}(x_j, \Delta\varphi')$] are the same irrespectively of the value of I_I and I_{II}. The values of x_L and x_U at the midspan section are listed in Table I versus $\Delta\varphi' \in [82°, 90°]$.

Complementary considerations can be made for the transition in convenience between phase in order and reverse phasing over subinterval [180°, 360°] (i.e., the transition from $B_{\rm ph} < B_{\rm rev}$ to $B_{\rm rev} < B_{\rm ph}$ over the whole section, occurring at $\Delta\varphi \sim 270°$). In this case, the calculations show the following.

TABLE I
LOWER EXTREME x_L AND UPPER EXTREME x_U OF THE RANGE OF DISTANCES FROM LINE AXIS WHERE THE TRANSITION IN CONVENIENCE BETWEEN PHASE IN ORDER AND REVERSE PHASING ($B_{\rm ph}(x_j, \Delta\varphi') < B_{\rm rev}(x_j, \Delta\varphi')$) AND VICE VERSA ($B_{\rm rev}(x_j, \Delta\varphi'') < B_{\rm ph}(x_j, \Delta\varphi'')$) OCCURS (AT 1 m ABOVE GROUND), VERSUS $\Delta\varphi' \in [82°, 90°]$ AND $\Delta\varphi'' \in [262°, 270°]$. MV TOWER LINE; MIDSPAN SECTION

Δφ'(°)	Δφ"(°)	x_L (m)	x_U (m)
82	262	+8.0	+22.0
83	263	+2.0	+28.0
84	264	−2.0	+36.0
85	265	−8.0	+44.0
86	266	−12.0	+52.0
87	267	−22.0	+64.0
88	268	−34.0	+82.0
89	269	−62.0	+100.0
90	270	−100.0	+100.0

a) The transition occurs at a progressively increasing number of field points in the midspan section, as $\Delta\varphi$ rises from 262° to 270°; at $\Delta\varphi = 270°$, the transition is complete (i.e., $B_{\rm rev} < B_{\rm ph}$ all over the line section). Let us call $\Delta\varphi''$ the values of $\Delta\varphi \in (262°, 270°)$ at which the transition takes place.
b) The extremes x_L and x_U of the range where the transition $B_{\rm rev}(x_j, \Delta\varphi'') < B_{\rm ph}(x_j, \Delta\varphi'')$ has already occurred for a given $\Delta\varphi$ " are independent of I_I and I_{II}, and are precisely the same already encountered in the previous transition for phase-shift angle values $\Delta\varphi' = \Delta\varphi'' - \pi$. These same values are listed in Table I versus $\Delta\varphi'' \in [262°, 270°]$ too.

Similar transitions in convenience of phase arrangements also take place at the tower section and/or at different heights of field points from the soil, even if with different values of x_L and x_U, and intervals of $\Delta\varphi'$ and $\Delta\varphi''$.

C. Synthetic Remarks About the NV Tower Line

The NV tower line of Fig. 4 has been carefully analyzed as done for the MV tower line, but detailed results are omitted here for the sake of brevity, since calculations lead to the same conclusions as the MV tower line. Indeed, statements 1.1–1.6 hold, on the whole, for the NV tower line. Hence, it can be argued that they are valid for whatever kind of tower structure and conductor height is chosen, provided that the phase conductors are arranged according to the phase in order scheme. Analogously, statements 2.1–2.6 hold, on the whole, also for the NV tower line. Hence, it can be argued that they are valid for whatever kind of tower structure and conductor height is chosen, provided that the phase conductors are arranged according to the reverse phasing scheme. However, the role played by conductor height has also to be checked carefully, particularly for low values of h_L.

Transitions in convenience between reverse phasing and phase-in-order arrangement, and vice versa, are also observed for the NV tower line, but with different intervals of $\Delta\varphi'$ and $\Delta\varphi''$, and different extremes of the range of field points where the transitions take place, with respect to the MV tower line. However, for both line structures (thus, likely, for all line

structures) and for all field point heights above the soil, the features of transitions do not depend on circuits currents.

An analysis of the phase-shift effects at heights above the ground other than 1 m (the value always assumed here) has also been performed for both line types, with particular emphasis put on heights from 1 to 10 m, typical of residential buildings of small-medium size. Such analysis is omitted here, both for the sake of brevity and since it confirms what is supported by intuition, namely that for a given tower structure and conductor arrangement, raising the field point height above the soil level at a fixed value of h_L is equivalent to lowering the value of h_L at a fixed field point height above the soil (if the ground behaves as a nonmagnetic nonconductive medium, as implied by assumptions 1 and 3 in Section II).

V. Conclusion

The extensive static analysis carried out above proves that the phase shift among current terns of the ac double-circuit transmission lines plays a crucial role on the magnetic field generated by such lines. The analysis also shows that the current phase-shift effects are often nonintuitive and hidden and, thus, should be studied properly by either extensive measurements or detailed calculations only, the latter being much cheaper and faster if a computer code like that shown here is available.

The static analysis, carried out for two-line tower topologies and two-phase arrangements (phase in order and reverse phasing) and repeated for several couples of rms phase currents, reveals interesting features of field profiles that are independent of current values, but depend only on the phase-shift angle; this gives rise to the concept of p.u.c. profiles. General statements about the overall behavior of such p.u.c. profiles as a function of phase-shift angle are then made, holding for a given phase arrangement whatever the tower structure is and/or the conductor height above the ground. Thus, the main conclusions drawn from this analysis for both the phase in order and the reverse phasing arrangement can be extended on the whole to different tower structures and conductor geometries of ACDOT lines, provided that the phase arrangement is the same.

It is also interesting to observe that a similar analysis, hence *mutatis mutandis* analogous considerations, can be applied to cases where more ac overhead transmission lines are in proximity with each other, though not on the same towers, and exhibit a phase shift among the relevant current phasor terns, thus adding a further perspective to this work.

As mentioned in Section I, the static analysis performed here is converted into a "dynamic" analysis in Part II of this investigation by applying the results of Part I to an existing line and to the relevant load-varying conditions over reference time periods lasting from one day to one year. Parts I and II confirm that current phase shifts of ac double-circuit transmission lines, either previewed at the design stage or indicated by line recordings, should be considered in magnetic-field calculation from such lines in order to avoid remarkable errors that may affect severe human exposure estimates.

Acknowledgment

The author would like to thank Dr. D. Andreuccetti of IFAC-CNR for contributions and providing the CAMPI code, Dr. A. Giorgi of TERNA-EnelGroup, and Dr. R. Conti of CESI and Dr. G. Petrini, for their precious technical support.

References

[1] B. M. Weedy and B. J. Cory, *Electrical Power Systems*, 4th ed. New York: Wiley, 1998.

[2] G. Mazzanti, "Current phase-shift effects in the calculation of magnetic fields generated by double-circuit overhead transmission lines," in *Proc. IEEE Power Eng. Soc. General Meeting*, Denver, CO, Jun. 6–10, 2004.

[3] IEEE Magnetic Fields Task Force, "Magnetic fields from electric power lines. Theory and comparison to measurements," *IEEE Trans. Power Del.*, vol. 3, no. 4, pp. 2127–2136, Oct. 1988.

[4] J. Swanson, "Magnetic fields from transmission lines: Comparison of calculations and measurements," in *Proc. Inst. Elect. Eng., Gen. Transm. Distrib.*, vol. 142, Sep. 1988, pp. 481–486.

[5] K. Hameyer, R. Mertens, and R. Belmans, "Numerical methods to evaluate the electromagnetic fields below overhead transmission lines and their measurement," in *Proc. 1st IEEE Int. Caracas Conf. Devices, Circuits Systems*, 1995, pp. 32–36.

[6] K. Yamazaki, T. Kawamoto, and H. Fujinami, "Requirements for power line magnetic field mitigation using a passive loop conductor," *IEEE Trans. Power Del.*, vol. 15, no. 2, pp. 646–651, Apr. 2000.

[7] M. A. Elhirbawy, T. T. Nguyen, L. Jennings, and W.W.L. Keerthipala, "Calculation of electromagnetic fields established by power transmission line using finite difference techniques," in *Proc. IEEE Canadian Conf. Electrical Computer Engineering*, vol. 1, 2002, pp. 311–316.

[8] A. R. Memari and W. Janischewskyi, "Mitigation of magnetic field near power lines," *IEEE Trans. Power Del.*, vol. 11, no. 3, pp. 1577–1586, Jul. 1996.

[9] A. S. Abdallah, "Electric fields from transmission lines nearby populated areas in Egypt: Theory vs experiment," in *Proc. 11th Int. Symp. High Voltage Engineering*, vol. 2, Aug. 1999, pp. 119–122.

[10] *Electric and Magnetic Fields Produced by Transmission System. Description of Phenomena and Practical Guide for Calculation*, 1980. CIGRE Working Group 36–01.

[11] *European Basic Standard on Measurements and Calculation Procedures for Human Exposure to Electric, Magnetic, and Electromagnetic Fields (0 Hz–300 GHz)*, 2004. European preStandard prEN 50 413.

[12] *IEEE Standard for Safety Levels With Respect to Human Exposure to Electromagnetic Fields, 0 to 3 kHz*

[13] R. Conti, A. Giorgi, R. Rendina, L. Sartore, and E. A. Sena, "Technical solutions to reduce 50 Hz magnetic fields from power lines," in *Proc. IEEE Bologna Power Tech. Conf.*, 2003.

[14] H. M. Ismail, "Magnetic field of high-phase order and compact transmission lines," *Int. J. Energy Res.*, vol. 26, pp. 45–55, Dec. 2001.

[15] M. Albano, R. Benato, and R. Turri, "Predictive analysis of environmental magnetic fields generated by multiple power lines," in *Proc. IEEE Bologna Power Tech. Conf.*, 2003.

[16] A. V. Mamishev, R. D. Nevels, and B. D. Russell, "Effects of conductor sag on spatial distribution of power line magnetic field," *IEEE Trans. Power Del.*, vol. 11, no. 3, pp. 1571–1576, Jul. 1996.

[17] A. Ahlbom *et al.*, "Guidelines for limiting exposure to time varying electric, magnetic and electromagnetic fields (up to 300 GHz)," *Health Phys.*, vol. 74, pp. 494–522, Apr. 1998. Int. Comm. Non-Ionizing Radiation Protection (ICNIRP).

[18] D. Andreuccetti, CAMPI-un programma per il calcolo del campo elettrico e del campo magnetico dispersi da elettrodotti ad alta tensione, (in Italian), in IFAC-CNR, May 2002. Version 4.1.

[19] N. Faletti and P. Chizzolini, *Trasmissione e Distribuzione Dell'energia Elettrica*, 6th ed. Bologna, Italy: Patron, 1992, vol. 2. (in Italian).

Giovanni Mazzanti (M'04) was born in Bologna, Italy, on July 12, 1962. He received the M.Sc. degree in nuclear engineering and the Ph.D. degree in electrical engineering from the University of Bologna, Bologna, Italy, in 1986 and 1992, respectively.

Currently, he is an Associate Professor of High-Voltage Engineering, University of Bologna. His research interests are life modeling, reliability, and diagnostics of high-voltage (HV) insulation, and human exposure to electromagnetic fields. He is the author or coauthor of many papers.